NASA TECHNICAL MEMORANDUM

NASA TM X-1622

NASA TM X-1622

OVERALL PERFORMANCE IN ARGON OF A 6-INCH RADIAL-BLADED CENTRIFUGAL COMPRESSOR

by Edward R. Tysl, Calvin L. Ball, Carl Weigel, and Laurence J. Heidelberg

Lewis Research Center
Cleveland, Ohio

NATIONAL AERONAUTICS AND SPACE ADMINISTRATION • WASHINGTON, D. C. • AUGUST 1968

NASA TM X-1622

OVERALL PERFORMANCE IN ARGON OF A 6-INCH RADIAL-BLADED CENTRIFUGAL COMPRESSOR

By Edward R. Tysl, Calvin L. Ball, Carl Weigel, and Laurence J. Heidelberg

Lewis Research Center
Cleveland, Ohio

NATIONAL AERONAUTICS AND SPACE ADMINISTRATION

For sale by the Clearinghouse for Federal Scientific and Technical Information
Springfield, Virginia 22151 – CFSTI price $3.00

ABSTRACT

Overall and impeller performance is presented as a function of equivalent weight flow. At the design equivalent weight flow of 1.52 pounds per second (0.69 kg/sec) and design equivalent tip speed of 989 feet per second (301.5 m/sec) the compressor developed an overall total pressure ratio of 2.3 with an adiabatic efficiency of 76.5 percent. Peak efficiency at design speed was 78.0 percent and occurred at an equivalent weight flow of 1.35 pounds per second (0.61 kg/sec).

OVERALL PERFORMANCE IN ARGON OF A 6-INCH RADIAL-BLADED CENTRIFUGAL COMPRESSOR

by Edward R. Tysl, Calvin L. Ball, Carl Weigel, and Laurence J. Heidelberg

Lewis Research Center

SUMMARY

A 6-inch (15.24-cm) radial-bladed centrifugal compressor applicable for a 10-kilowatt Brayton cycle space power system was tested in argon at an inlet pressure of 6 pounds per square inch absolute (41.36×10^3 N/m^2 abs). Both overall performance and impeller performance is presented as a function of equivalent weight flow and a comparison with the predicted performance is made.

At the design equivalent weight flow of 1.52 pounds per second (0.69 kg/sec) and design equivalent tip speed of 989 feet per second (301.5 m/sec), the compressor developed an overall total pressure ratio of 2.30 and an adiabatic efficiency of 0.765. At design speed the peak pressure ratio was 2.35 and the peak efficiency was 0.78. The peak values occurred at an equivalent weight flow of 1.35 pounds per second (0.61 kg/sec). As the speed was reduced from the design value to 50 percent of design, the peak efficiency increased from 0.78 to about 0.82.

INTRODUCTION

As the duration of space missions increases, continuous onboard generation of electrical power over periods of thousands of hours will be required. Power requirements can be expected to range from a few kilowatts for vehicles requiring relatively small amounts of auxiliary power to many megawatts for vehicles using electric propulsion in space. For small power systems, the Brayton cycle inert gas system is of interest.

Studies of Brayton cycle systems have shown that weight of turbomachinery components is relatively insignificant in system optimization. However, component efficiencies have a strong effect on the size and weight of the heat-supply and heat-rejection components (refs. 1 and 2). Thus turbomachinery research effort should logically be directed towards improving component efficiency with weight secondary and size impor-

tant only as it affects ease of packaging components in a vehicle.

The effect on component performance of dimensional scaling of aircraft turbine engine components to the sizes required for small space power systems is not well established. Thus it is necessary to investigate components in the size required to determine that acceptable efficiencies can be attained.

The present investigation was conducted to obtain a performance level for a radial-bladed centrifugal compressor in a size suitable for application in a 10-kilowatt Brayton cycle power system. The compressor was designed for use in argon gas which is one of the working fluids considered for the Brayton cycle space power system (refs. 1 and 2). The compressor design and fabrication (ref. 3) was accomplished by contract to the AiResearch Manufacturing Company, Division of the Garrett Corporation, Phoenix, Arizona.

Preliminary testing was conducted at the contractor's plant for proof of mechanical integrity and determination of the impeller leading edge trim and diffuser vane setting angle required to achieve an acceptable flow range with respect to design weight flow. All performance data reported herein were obtained in tests at the NASA Lewis Research Center.

SYMBOLS

a	stagnation speed of sound, ft/sec (m/sec)
c_p	specific heat at constant pressure of argon, 0.125 Btu/(lb)($^{\circ}$R); 523.759 J/(kg)(K)
D	diameter, ft (m)
f_{cw}	compressor work factor, $gJc_p(T_6 - T_1)/U_{t3}^2$
f_s	slip factor, $V_{ut3}/U_{t3} = gJc_p\,\Delta T_{vd}/U_{t3}^2$
f_w	windage factor, $gJc_p\,\Delta T_w/U_{t3}^2$
g	gravitational acceleration, 32.17 ft/sec^2 (9.807 m/sec^2)
H	ideal head rise, ft (m)
J	mechanical equivalent of heat, 778.16 (ft)(lb)/Btu; 0.999 (m)(N)/J
N_s	specific speed, $RPM\sqrt{Q}/60(gH)^{3/4}$
P	total (stagnation) pressure, psia (N/m^2 abs)
p	static pressure, psia (N/m^2 abs)

Q	argon volume flow, ft^3/sec (m^3/sec)
R	gas constant, argon = 38.683 ft-lb/(lb)(^oR); 208.127 (m)(N)/(kg)(K)
Re	Reynolds number, $\rho_1 U_{t3} D_{t3}/\mu_1$
RPM	impeller rotational speed, rpm
T	total (stagnation) temperature, ^oR (K)
ΔT_{vd}	gas temperature rise associated with vector diagrams, ^oR (K)
ΔT_w	gas temperature rise associated with windage, ^oR (K)
U	impeller wheel speed, ft/sec (m/sec)
V	absolute gas velocity, ft/sec (m/sec)
W	weight (mass) flow rate, lb/sec (kg/sec)
γ	ratio of specific heat at constant pressure to specific heat at constant volume, c_p/c_v, for argon 1.667
δ	ratio of compressor inlet total pressure to NASA standard sea level pressure, $P_1/14.7$ psia ($P_1/101.35\times10^3$ N/m^2 abs)
η	adiabatic temperature rise efficiency, $T_1\left[(P_6/P_1)^{(\gamma-1)/\gamma} - 1\right]\Big/(T_6 - T_1)$
θ	ratio of compressor inlet total temperature to NASA standard sea level temperature, $T_1/518.7^o$ R ($T_1/288.17$ K)
μ	dynamic viscosity, 1.49×10^{-5} lb/(sec)(ft) at 518.7° R; 2.217×10^{-5} (N)(sec)/m at 288.17 K
ρ	density, 0.1055 lb/ft^3 at 518.7° R and 14.7 psia; 1.690 kg/m^3 at 288.17 K and 101.35×10^3 N/m^2 abs

Subscripts:

m	meridional component
t	tip
u	tangential component
1	station in inlet pipe 5 in. (12.7 cm) upstream of compressor inlet flange (fig. 9)
2	station at impeller inlet (fig. 9)
3	station at impeller outlet (fig. 9)
4	station at diffuser blade inlet (fig. 9)
5	station at diffuser blade outlet (fig. 9)

6 station in exit pipe 3 in. (7.62 cm) downstream of compressor scroll exit flange (fig. 9)

Superscript:

' relative to impeller

COMPRESSOR DESIGN

The compressor was designed to fit a specific closed Brayton cycle system. It was designed for optimum performance with argon as the working fluid. The values of the compressor design parameters and the equivalent values for standard inlet conditions are given in table I. A detailed description of the procedure employed in arriving at the final design point values is given in reference 3. A summary of the design is presented herein.

TABLE I. - VALUES OF COMPRESSOR DESIGN PARAMETERS

(WORKING FLUID - ARGON)

Compressor design parameters	Based on design inlet pressure and temperature	Based on standard inlet pressure and temperature
Inlet total pressure, P_1, psia (N/m^2 abs)	6 (41.36×10^3)	14.7 (101.35×10^3)
Inlet total temperature, T_1, ^oR (K)	536 (297.78)	518.7 (288.17)
Weight flow rate, W, lb/sec (kg/sec)	0.611 (0.278)	1.52 (0.69)
Compressor total pressure ratio, P_6/P_1	2.38	2.38
Compressor total temperature ratio, T_6/T_1	1.525	1.525
Compressor efficiency, η_{1-6}	0.798	0.798
Impeller total pressure ratio, P_3/P_1	2.62	2.62
Impeller efficiency, η_{1-3}	0.896	0.896
Rotative speed, rpm	38 500	37 900
Impeller tip speed, U_{t3}, ft/sec (m/sec)	1004 (306)	989 (301.5)
Impeller slip factor, f_s	0.830	0.830
Impeller windage factor, f_w	0.039	0.039
Compressor work factor, f_{cw}	0.869	0.869
Specific speed, N_s	0.1057	0.1057
Reynolds number, Re	13×10^5	34.7×10^5

Impeller Design

Fifteen blades were chosen for the impeller. The impeller exit diameter required to satisfy the compressor design values was calculated to be 5.976 inches (15.179 cm). The impeller exit blade height was set at 0.217 inch (0.551 cm). Impeller inlet dimensions were selected based on the desired inlet flow conditions and their relation to the exit diameter for good impeller efficiencies. The impeller inlet tip diameter was set at 3.528 inches (8.961 cm) and the hub diameter at 1.858 inches (4.719 cm). Design velocity diagrams for the impeller inlet and the impeller outlet are shown in figure 1.

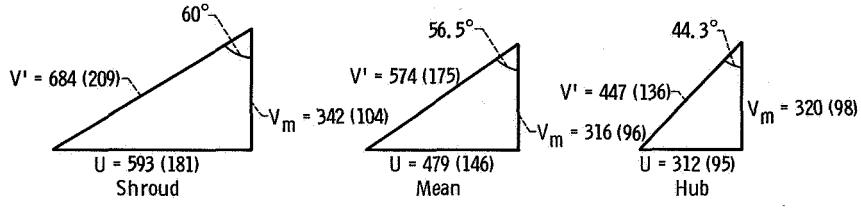

(a) Impeller inlet (station 2).

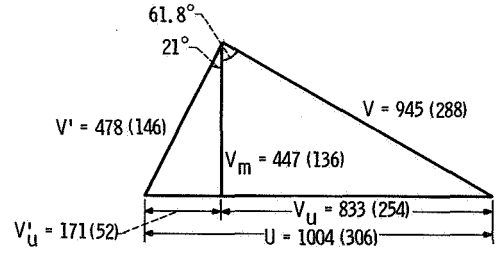

(b) Impeller exit (station 3).

Figure 1. - Impeller design velocity diagrams. (All dimensions in feet per second (m/sec) unless indicated otherwise.)

A computer program which calculates the impeller internal flow velocities based on the analysis method given in reference 4, appendix A was employed in the impeller channel design. The blade shape and the hub and shroud contours were adjusted until satisfactory velocity and pressure distributions were achieved within the impeller channel. The design velocity distributions are shown in figure 2.

As noted in table I a work factor is listed for the compressor along with an impeller slip factor. The compressor work factor is defined as being equal to the slip factor plus a windage factor and is given by the following equation:

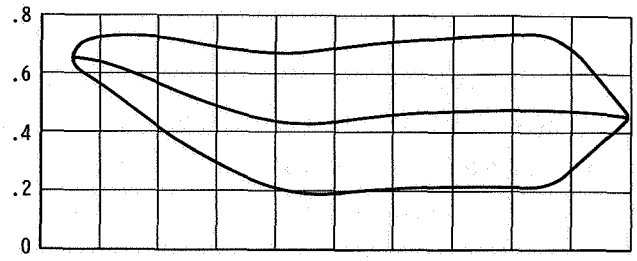

(a) Shroud streamline. Approximate length, 2.5 inches (6.35 cm).

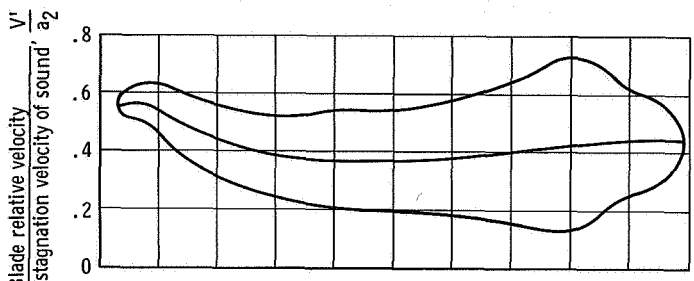

(b) 50 Percent streamline. Approximate length, 2.96 inches (7.52 cm).

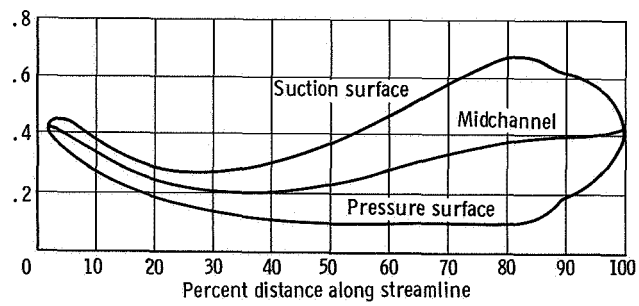

(c) Hub streamline. Approximate length, 3.34 inches (8.48 cm).

Figure 2. - Compressor impeller velocity distribution.

$$f_{cw} \equiv f_s + f_w = \frac{gJc_p\,\Delta T_{vd}}{U_{t3}^2} + \frac{gJc_p\,\Delta T_w}{U_{t3}^2} = \frac{gJc_p(\Delta T_{vd} + \Delta T_w)}{U_{t3}^2} = \frac{gJc_p(T_6 - T_1)}{U_{t3}^2}$$

The slip factor is based on the gas temperature rise due to the energy addition associated with the vector diagrams, and the windage factor is based on the gas temperature rise due to the windage at the back face of the impeller and between the impeller vanes and stationary shroud. The compressor work factor is based on the measured temperature rise which includes both the temperature rise due to the vector diagram energy addition and the temperature rise due to windage.

Diffuser and Scroll Design

A short vaneless diffuser, about 0.10 inch (0.254 cm) in the radial direction, was used between the impeller exit and diffuser vane inlet. The diffuser vane shapes were designed to give a smooth deceleration on both suction and pressure surfaces.

Design velocity diagrams at diffuser vane inlet and exit are shown in figure 3. The calculated velocity distribution along the diffuser vane surface is shown in figure 4.

The scroll was designed with essentially circular cross sections which were located to blend with the diffuser flow passage. The circumferential variation in cross-sectional area was selected based on satisfying the condition of constant angular momentum and continuity of mass flow. The design Mach number at the compressor exit flange was 0.16.

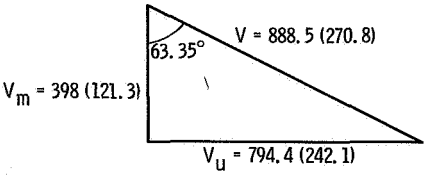

(a) Diffuser inlet diagram (station 4) based on effective flow area which includes vane leading edge blockage.

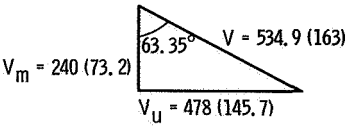

(b) Diffuser exit diagram (station 5) based on core flow conditions.

Figure 3. - Diffuser design velocity diagrams. (All dimensions in feet per second (m/sec) unless otherwise indicated.)

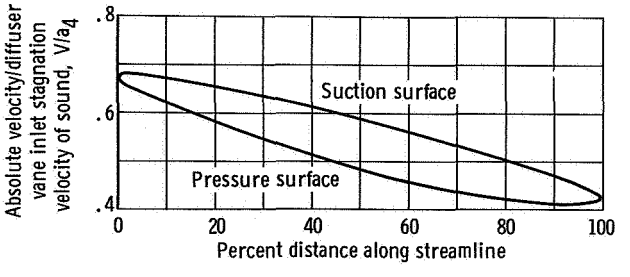

Figure 4. - Diffuser blade velocity distribution. Approximate streamline length, 1.69 inches (4.29 cm).

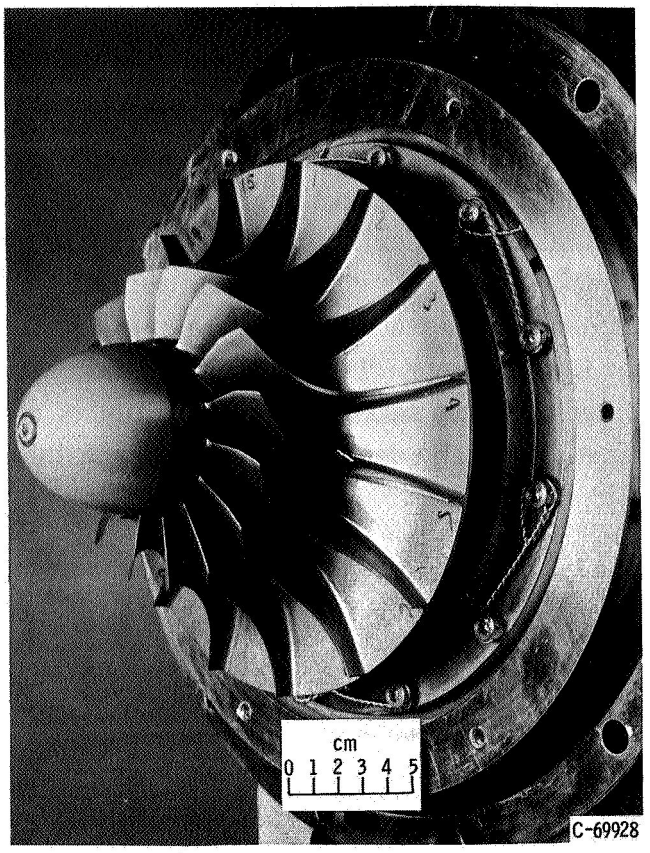

Figure 5. - Centrifugal impeller.

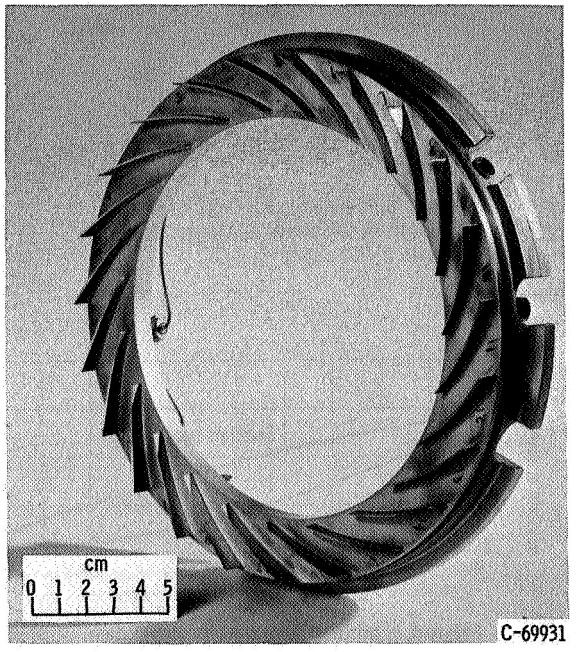

Figure 6. - Vaned diffuser.

Preliminary experimental tests conducted by the contractor using the design configuration compressor required an adjustment to the diffuser vane angle in order to more closely approach the design pressure ratio at design weight flow. The final compressor configuration utilized diffuser vanes having an angle setting 3^{o} less than the design angle as measured from the radial direction. The diffuser vane design velocity diagrams and velocity distribution (fig. 4) were not modified to account for the change in diffuser vane setting angle.

APPARATUS AND PROCEDURE

Test Apparatus

The impeller used in this investigation was machined from a titanium forging and is shown in figure 5. Figure 6 is a photograph of the vaned diffuser located downstream of the impeller. The vaned diffuser has 23 blades which are integral with the vaned diffuser blade ring and were machined from 347 stainless steel material. The diffuser vane tips

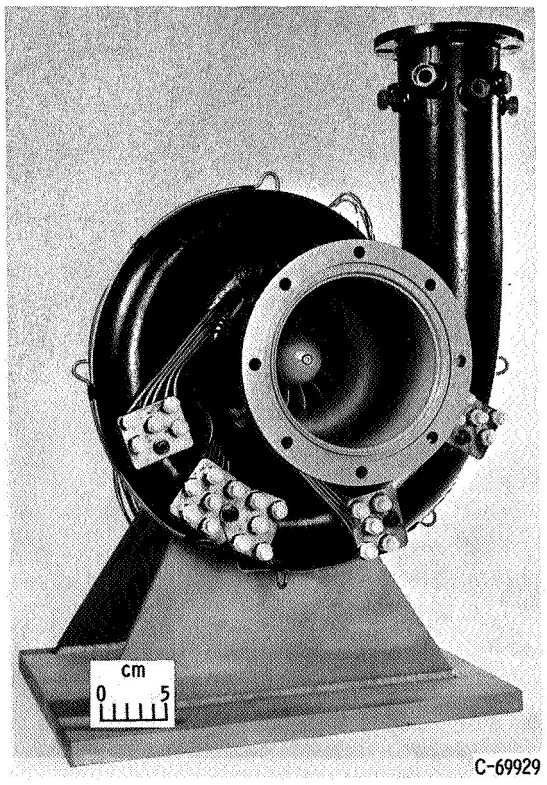

Figure 7. - Centrifugal compressor package.

were contoured to fit the machined aluminum casting that comprised the compressor scroll, impeller shroud, and inlet. This casting is shown in figure 7, which is a photograph of the complete compressor package prior to facility installation.

The compressor drive unit consisted of a single-stage axial flow air turbine. The turbine was connected to the compressor package by a high-speed coupling. Turbine speed was controlled by a remotely operated electropneumatic valve. These components are shown assembled and alined on the bedplate table in figure 8.

The compressor package consisted of the aerodynamic hardware, bearing-seal shaft assembly, and stand. A cutaway view of the compressor package is shown in figure 9. Included in the figure are the location of instrumentation and calculation stations. The compressor impeller was cantilever mounted on a shaft supported by two angular contact bearings. Carbon face seals outboard of each bearing were utilized to prevent bearing oil leakage. A carbon shaft seal was installed between the compressor im-

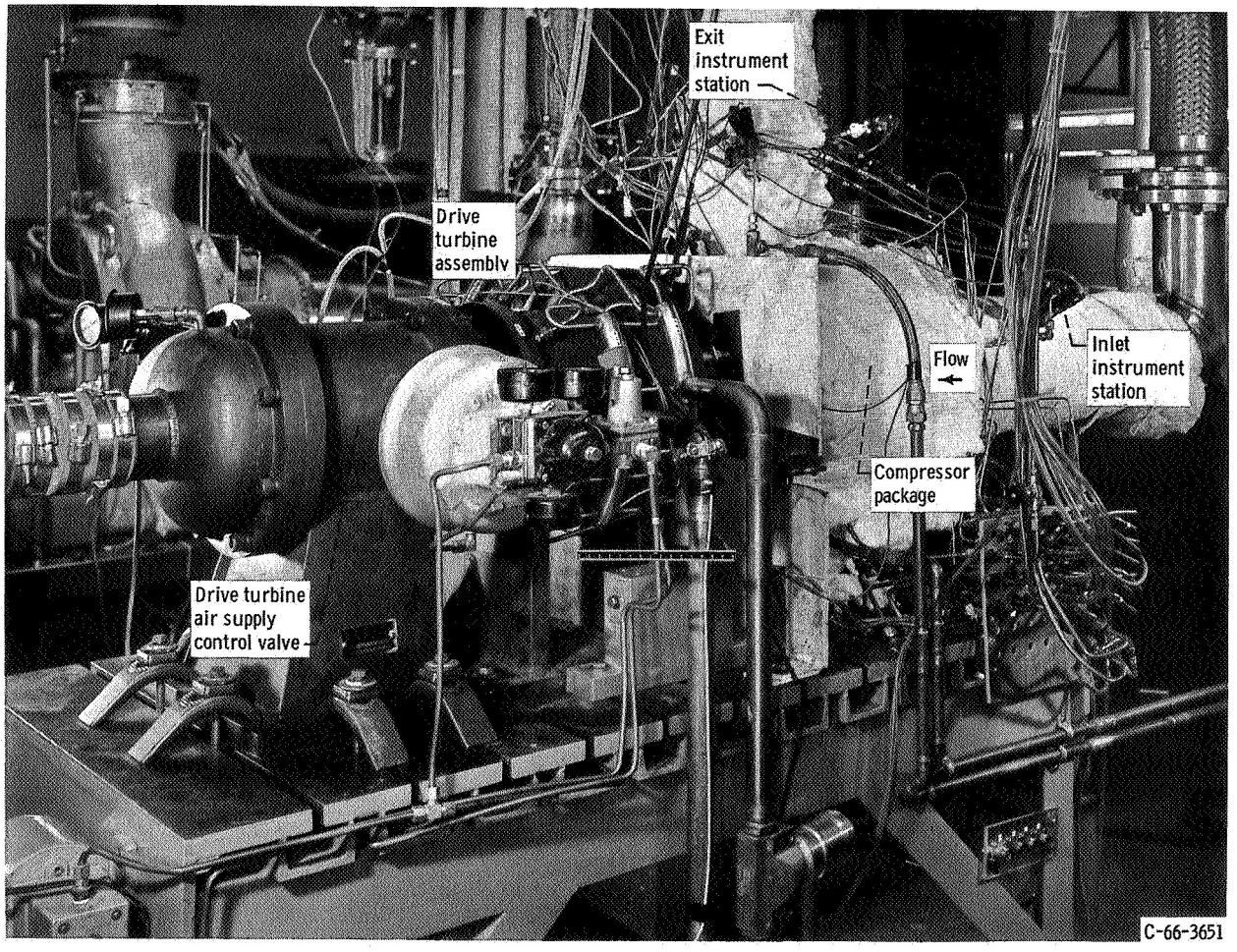

Figure 8. - Component assembly.

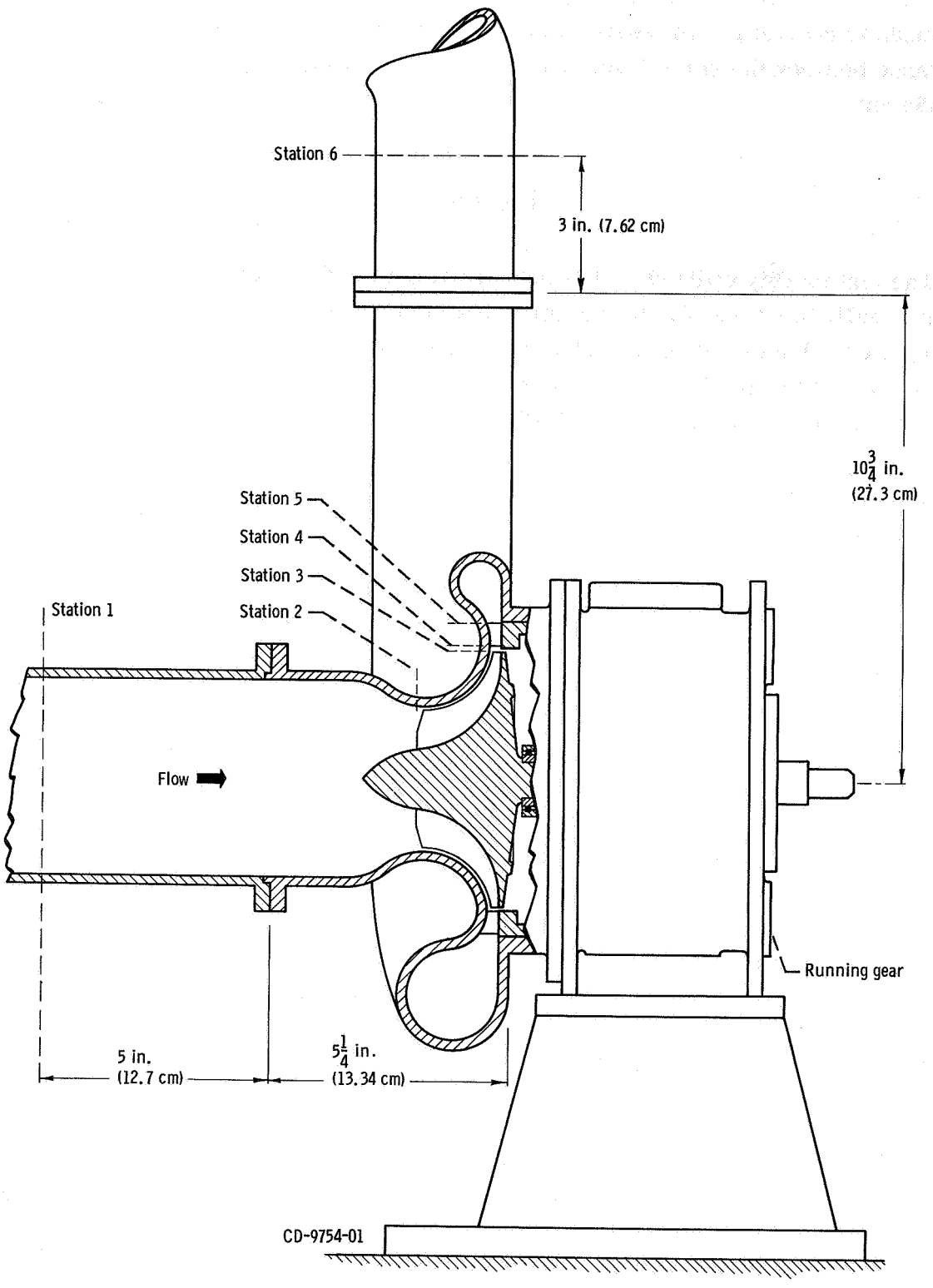

Figure 9. - Compressor package.

peller and carbon face oil seal to ensure argon purity in the test facility. Provision was made to control gas pressure in the cavity between these seals. The static impeller clearance between the shroud and blade tip at impeller discharge was set at 0.010 inch (0.0254 cm).

Test Facility

The test facility utilized in this investigation is of the open loop type and is shown schematically in figure 10. In this investigation high-purity argon gas (contaminants $\leq$50 ppm by volume) was used. The argon supply consisted of gas trailers located outside of the test facility building. Automatic temperature controls for the 25-kilowatt electric heater maintained the required compressor inlet temperature. A remotely operated pressure control valve was used to maintain compressor inlet pressure. Compressor gas flow and exit pressure were regulated by an electrically operated butterfly valve and a remote pneumatic operated globe valve installed in parallel in the exhaust piping downstream of the research compressor. The globe valve was used as a vernier

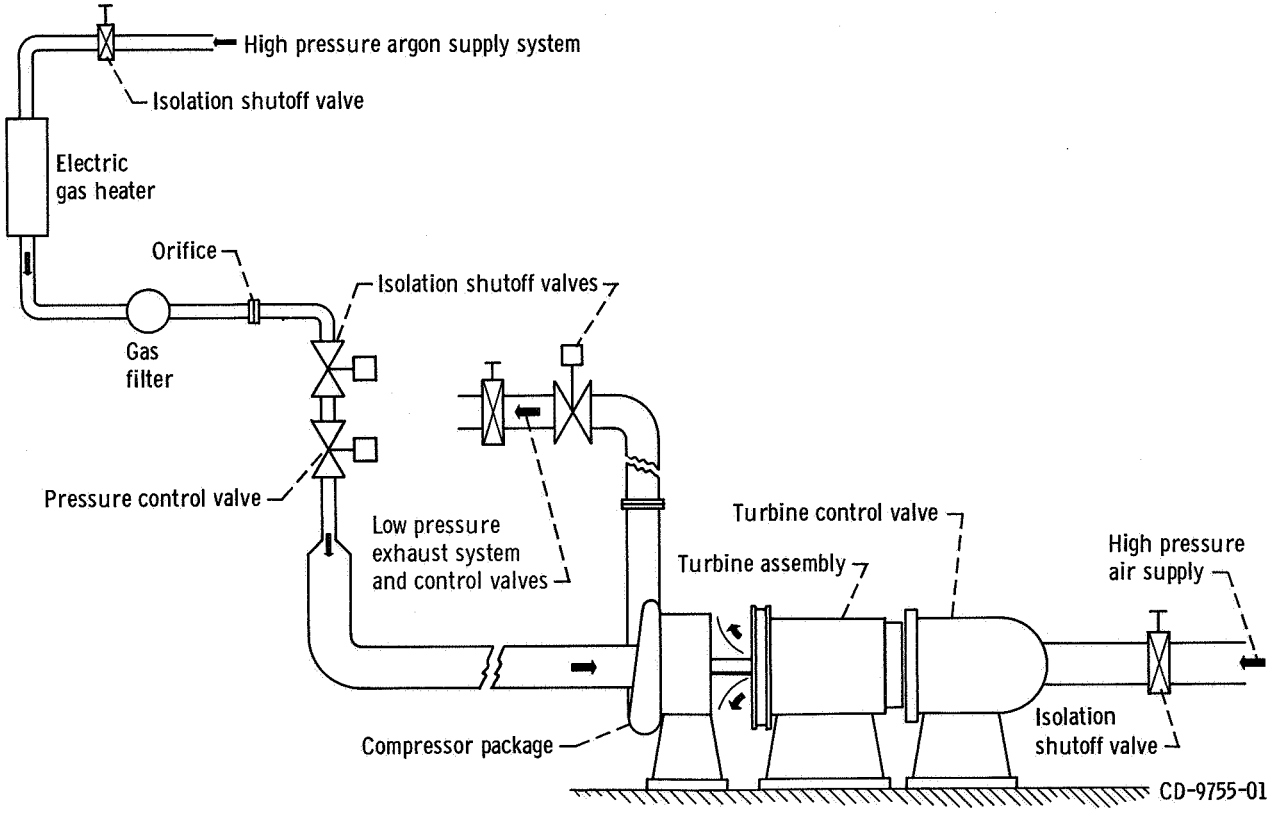

Figure 10. - Compressor test facility.

flow control valve to enable the facility operator to make small adjustments in compressor flow rate. The laboratory exhaust system carried the compressor gas flow to the atmosphere.

The laboratory dry air supply capable of furnishing dry air at several pressure levels was used as air supply source for the drive turbine. Air flow to the drive turbine was controlled by a modulated pneumatic valve. An automatic overspeed shutdown circuit was installed in the speed indicating system.

Instrumentation

Flow through the compressor was determined from a thin-plate orifice installed according to ASME standards in the compressor gas supply line (fig. 10). Overall compressor performance was computed from total pressures and total temperatures obtained at the compressor inlet and exit instrumentation stations 1 and 6 (fig. 9).

A sketch of the compressor inlet and exit instrumentation is presented in figure 11. At station 1 the instrumentation consisted of three wall static pressure taps equally spaced around the circumference and three combination total pressure-temperature rakes. The total pressure heads on the rakes were located radially at the centers of

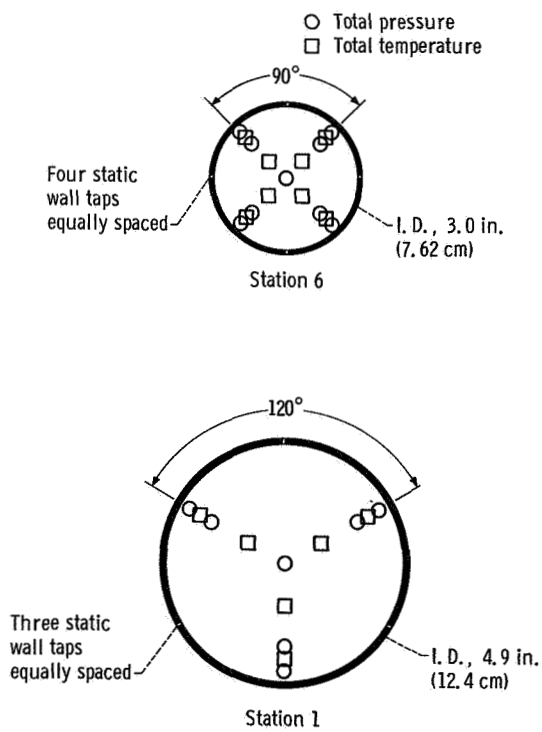

Figure 11. - Instrumentation at stations 1 and 7.

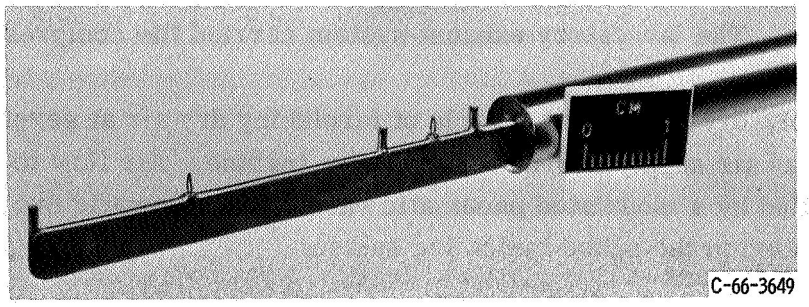

Figure 12. - Combination total pressure and total temperature rake.

three equal annular areas and the spike-type iron-constantan thermocouples were placed midway between the total pressure heads. A photograph of one of the inlet station combination rakes is presented in figure 12.

The compressor exit flow conditions (station 6, fig. 9) were measured with four wall static pressure taps equally spaced around the circumference and four combination total pressure-temperature rakes. The exit rakes were similar in design to the inlet station combination total pressure-temperature rakes.

Compressor static and total pressures were measured on a 100-inch (254-cm) mercury manometer board, recorded on film, and read to an accuracy of ±0.05 inch (0.13 cm) of mercury. All other data were measured by an automatic digital potentiometer and recorded on paper tape. The pressure drop across the thin-plate orifice and orifice inlet pressure were measured with strain-gage-type transducers. The pressure ranges of these transducers were selected to maintain a pressure measuring accuracy within ±1.5 percent. Gas temperatures were measured by spike-type thermocouples with an estimated accuracy of $\pm 1.5^{\circ}$ R (±0.8 K).

Compressor speed was indicated with the use of a magnetic pickup in conjunction with a gear mounted on the compressor shaft. In order to maintain constant compressor speed during test operations, an electronic control circuit was used in conjunction with the pneumatic controls for regulating drive turbine air flow. This control circuit was capable of automatically maintaining compressor speed within ±1/2 percent of the speed set by the test facility operator.

Test Procedure

Compressor test data were taken over a range of weight flows from maximum flow to stall conditions, at each of the following speeds: 50, 60, 70, 90, and 100 percent equivalent design speed. Data were not obtained at the 80 percent speed level because of a facility drive turbine vibration problem.

Throughout the test series, inlet pressure and inlet temperature were maintained at nominal design conditions of 6 pounds per square inch absolute and 536° R (41.36×10^3 N/m^2 abs and 297.8 K), respectively.

Analysis Calculation Procedure

The total pressure ratio and temperature rise efficiency for the compressor package (overall performance, stations 1 to 6, fig. 9) and compressor work factor were calculated based on the equations defined in the symbol list and measured pressures and temperatures. The total pressure ratio and temperature rise efficiency for the impeller (impeller performance, stations 1 to 3, fig. 9) was determined based on a calculated total pressure at the impeller exit (station 3, fig. 9). Total pressure at the impeller exit was not measured because of space limitations. In calculating the total pressure at the impeller exit, P_3, it was necessary to first calculate the total pressure at the diffuser vane inlet, P_4, where a measurement of static pressure was made. The total pressure at station 3 was determined by relating it to the calculated total pressure at station 4 through a design loss coefficient. The detailed procedure employed in calculating P_3 is presented in appendix A.

RESULTS AND DISCUSSION

The data presented herein were obtained from a 5.976-inch (15.179-cm) diameter radial-bladed centrifugal compressor operated in argon.

Overall Performance

The overall performance is presented in figure 13. Total pressure ratio and adiabatic efficiency as a function of argon weight flow is presented for five speeds. At the equivalent design tip speed of 989 feet per second (301.5 m/sec) and design equivalent weight flow of 1.52 pounds per second (0.69 kg/sec), the compressor produced a total pressure ratio of 2.30 with an adiabatic efficiency of 0.765 (fig. 13). The design pressure ratio was 2.38 with a predicted efficiency of 0.798. As weight flow was decreased at design speed to 1.35 pounds per second (0.61 kg/sec) both pressure ratio and adiabatic efficiency increased to peak values of 2.35 and 0.78, respectively. As weight flow was further decreased to the near stall condition of 1.23 pounds per second (0.56 kg/sec), both total pressure ratio and efficiency decreased slightly to values of 2.34

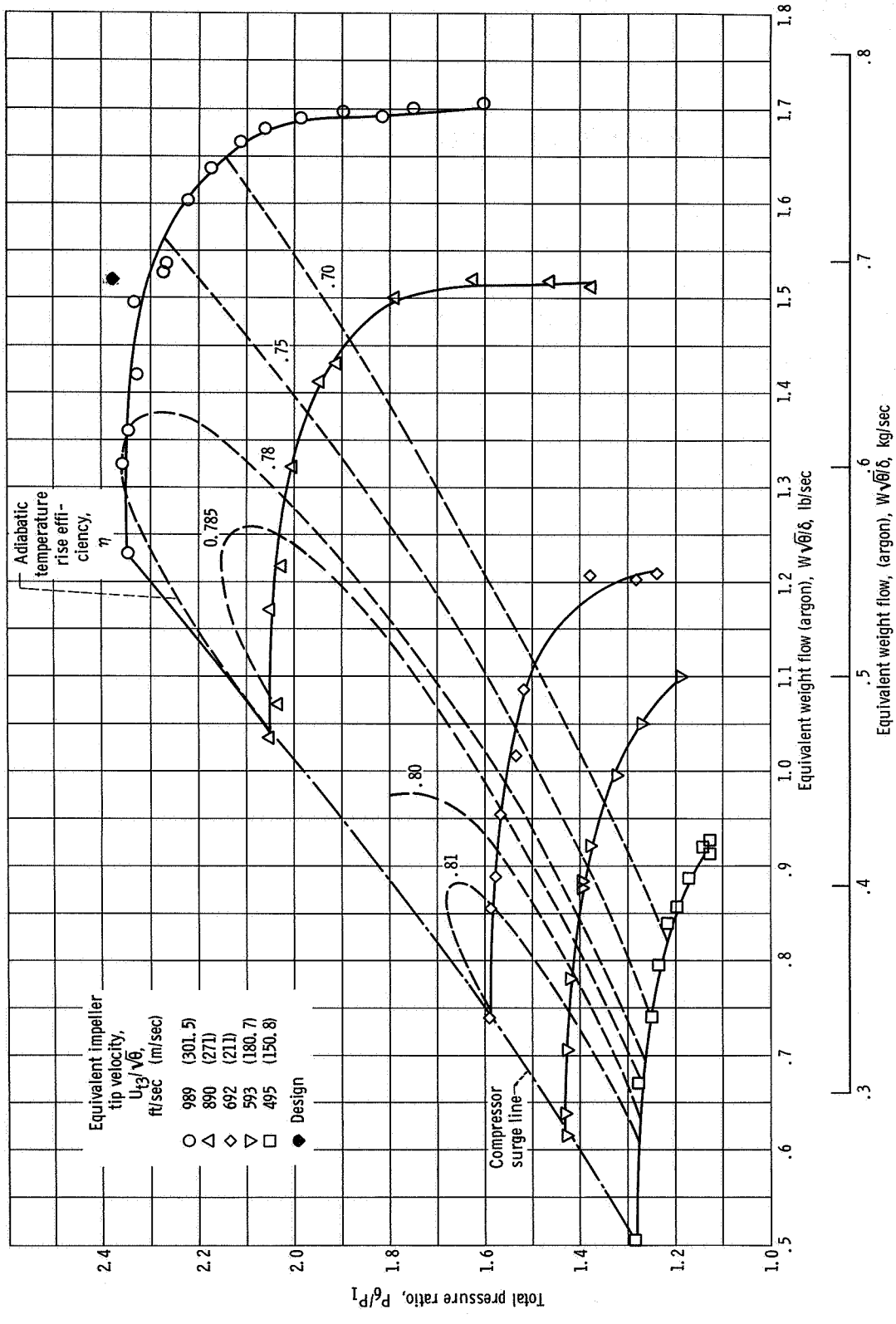

(a) Pressure ratio as a function of weight flow.

Figure 13. - Overall performance of 6-inch (15.24-cm) radial-bladed centrifugal compressor.

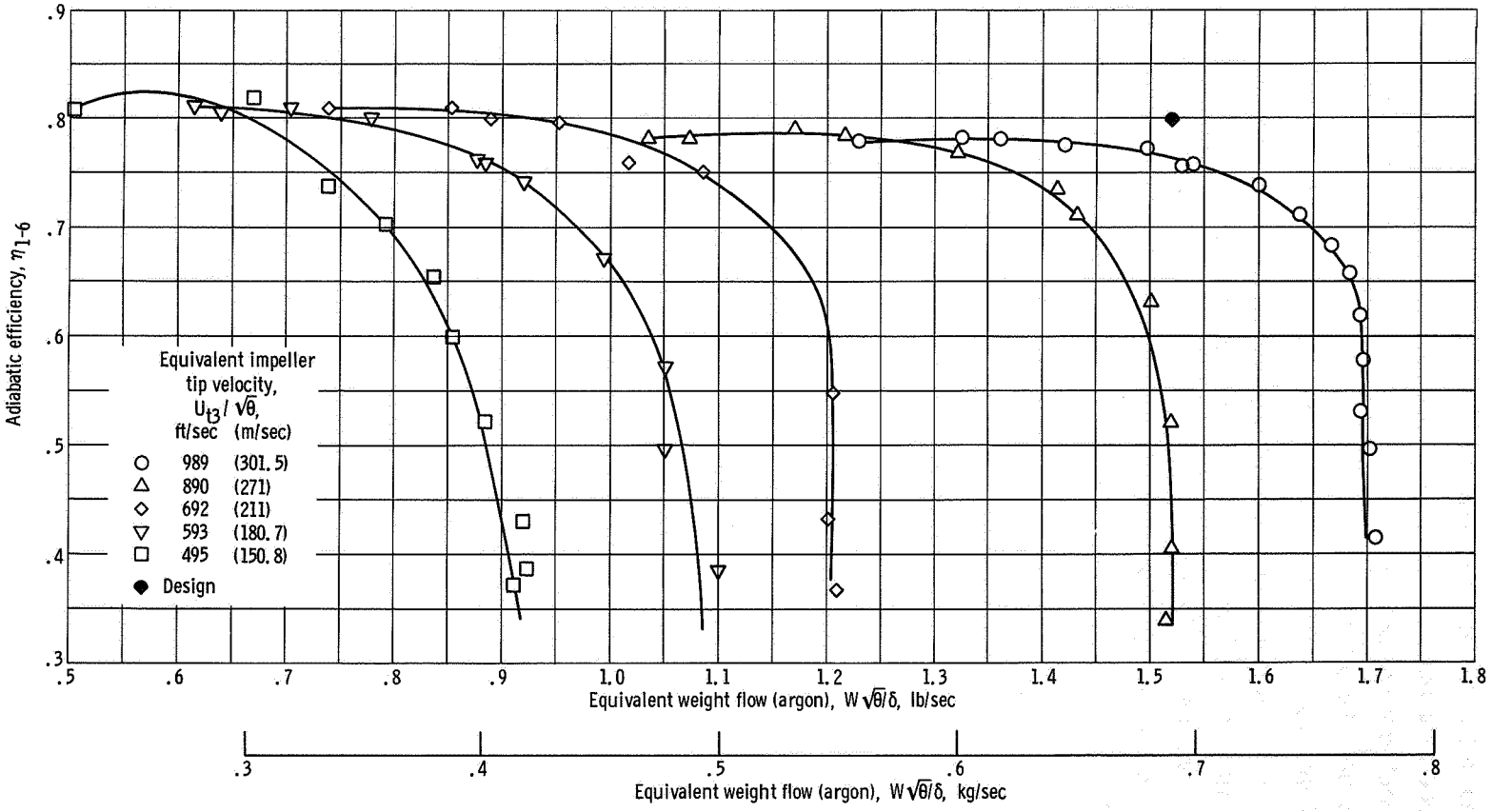

(b) Efficiency as a function of weight flow.

Figure 13. - Concluded.

and 0.775, respectively. Similar performance curves were obtained at the lower speeds. As indicated in figure 13, the peak efficiency increased with decreasing speed from 0.78 at design speed to about 0.82 at 50 percent design speed.

The data presented were obtained from the operation of the compressor completely insulated with 4 inches (10.16 cm) of fiberglass. The insulation was extended to and beyond instrument stations 1 and 6 located outside of the compressor package (fig. 9). A phenolic shim was employed between the compressor package support structure and the bedplate to act as a heat block. In spite of all efforts to prevent heat transfer during compressor tests, two potential heat leak paths remained. These were (1) heat transfer from impeller outlet to impeller inlet via the stationary aluminum shroud and (2) heat loss to compressor bearing oil supply. Calculations to determine the effect on compressor efficiency by each of the two heat transfer conditions were made at the compressor design speed and design flow operating point. The calculation involving the

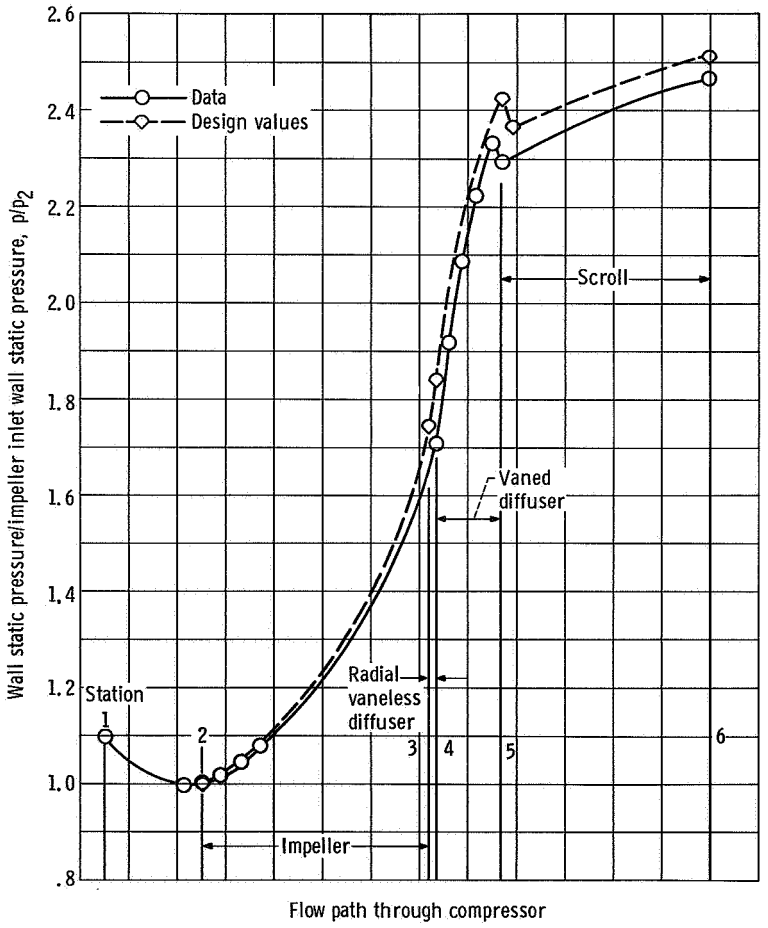

Figure 14. - Static pressure distribution at design speed and flow. Equivalent weight flow, 1.529 pounds per second (0.694 kg/sec); equivalent impeller tip velocity, 989 feet per second (301.5 m/sec).

heat transfer to the compressor inlet indicates that this process (similar but opposite to that of intercooling) degrades compressor efficiency by about three-fourths of a point. The experimental efficiency presented herein includes the effect of the recirculation of heat within the compressor. If a shroud made of a different material and thickness (e.g., stainless steel) were substituted for the aluminum shroud, a gain in efficiency might be possible. The calculation of heat loss from the compressor argon flow to the bearing oil supply indicates that compressor efficiency as calculated from a measured gas temperature rise (and presented herein) is about one point higher than the true adiabatic efficiency. Thus the analysis of the two potential heat leak paths and how they may affect the compressor temperature rise efficiency indicates that the magnitude of each is about the same but in opposite directions such that they appear to cancel each other in this particular study.

Static pressure rise through the compressor is shown in figure 14 at design speed and near equivalent design flow rate. Design static pressure values at several stations are also indicated in the figure. The difference between measured and predicted values of static pressure throughout the compressor appears to be primarily due to a lower than design static pressure rise in the impeller. This indicates that the losses for the impeller were higher than design and/or that the true effective flow area is less than that assumed in the design.

Calculated Impeller Performance

Calculated impeller total pressure ratio and adiabatic efficiency at design speed are presented in figure 15. The procedure employed in calculating the impeller pressure ratio and efficiency was in accordance with that presented in the calculation procedure section and appendix A. The design effective flow areas of 0.86 and 0.95 of the actual flow areas were assumed for the impeller exit and diffuser vane inlet, respectively, in calculating the impeller performance presented in figure 15. These effective flow areas were calculated from the design vector diagrams and measured passage widths. The impeller total pressure ratio at equivalent design flow of 1.52 pounds per second (0.69 kg/sec) was calculated to be 2.44. The impeller efficiency at design flow was calculated to be 0.83. The design values of pressure ratio and efficiency are 2.62 and 0.896, respectively. Since the calculated values are considerably below the design, it appears likely that the effective flow area at the impeller discharge is less than design. (A decrease in assumed effective flow area would result in a higher calculated pressure ratio and efficiency for the impeller.)

To determine the sensitivity of impeller performance with respect to effective flow area, the impeller performance at design flow was calculated assuming a decrease in

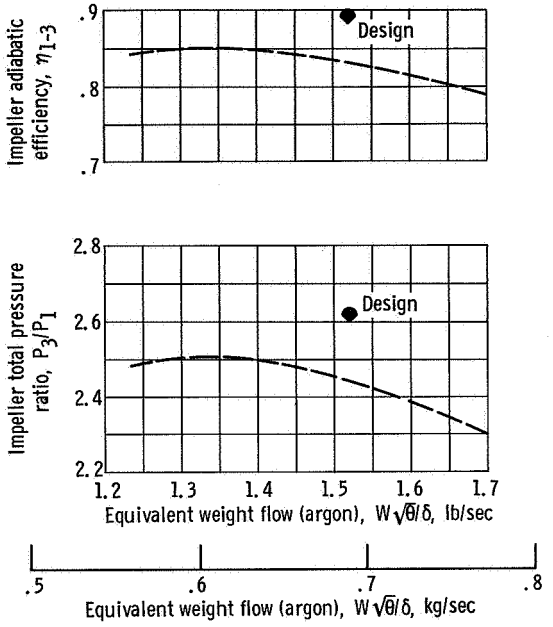

Figure 15. - Calculated impeller performance at design speed with assumed blockage.

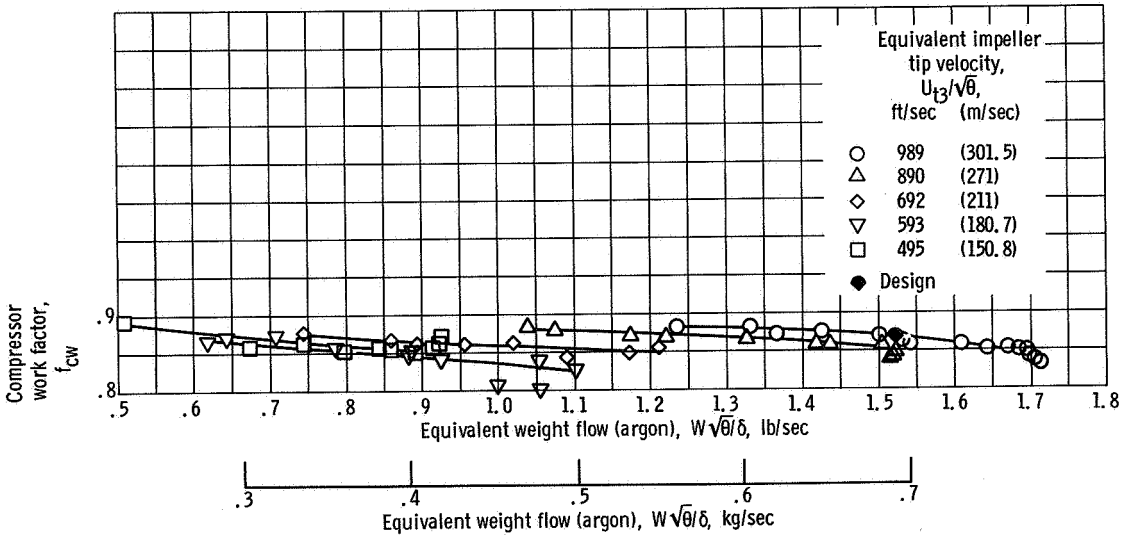

Figure 16. - Compressor work factor plotted against equivalent weight flow.

effective flow area of 15 points at both the impeller exit and diffuser vane inlet (effective flow areas of 0.71 and 0.80, respectively, of the actual flow areas). The lower effective flow areas resulted in an increase in the calculated impeller pressure ratio and efficiency from 2.44 to 2.55 and 0.83 to 0.87, respectively. The aforementioned calculations indicate that the actual effective flow area was probably less than design and the total pressure loss was probably somewhat greater than design.

The calculated absolute flow angles at the diffuser vane inlet were approximately 3° lower than design (as measured from the radial direction) with the assumed design effective flow area. For the case of decreased effective flow area, the calculated flow angle was 6° lower than design. These decreases in flow angle result from the higher through flow velocities associated with the lower impeller exit pressures. As discussed earlier in this report, to obtain an acceptable flow range with respect to design weight flow, it was necessary to adjust the diffuser vane setting angle to 3° less than design. This required adjustment in diffuser vane setting angle is further evidence that the impeller efficiency and effective flow area were lower than design.

Experimental compressor work factors for 50, 60, 70, 90, and 100 percent design speed are presented in figure 16. The compressor work factor compares favorably with the design value. This indicates that the design energy input to the gas was achieved.

Both peak impeller performance and peak overall compressor performance occur at a weight flow lower than the design value as shown in figures 13 and 15. The fact that peak performance values approach design values indicates that with adjustment in impeller leading edge trim and diffuser vane setting angle, near design performance can be obtained at design flow.

CONCLUDING REMARKS

A 6-inch (15.24-cm) diameter radial-bladed centrifugal compressor suitable for a 10-kilowatt solar Brayton cycle power generation system was tested in argon. The data presented include overall performance and calculated impeller performance. An overall peak adiabatic efficiency of 0.78 with a corresponding pressure ratio of 2.35 was obtained at design speed. At design speed and design flow rate, a total pressure ratio of 2.30 and an adiabatic efficiency of 0.765 were measured. These values were lower than the predicted values of 2.38 and 0.798, respectively. The experimental value of compressor work factor compares favorably with the design value. The difference between actual and predicted overall performance appears to be partly due to higher than predicted losses within the impeller. Improvement in performance at design speed and

weight flow condition might be obtained by an adjustment of the diffuser vane setting angle/or adjustment in impeller leading edge trim,

Lewis Research Center,
National Aeronautics and Space Administration,
Cleveland, Ohio, April 9, 1968,
120-27-03-06-22.

APPENDIX - ANALYSIS CALCULATION PROCEDURE

To determine the total pressure at the impeller exit, P_3, and thus impeller performance, it was necessary to first determine the total pressure at the diffuser vane inlet, P_4. Total pressure P_4 can be calculated utilizing the measured static pressure at station 4. With the total temperature at the impeller exit, T_3, and diffuser vane inlet, T_4, assumed equal to that measured at the compressor exit, T_6, the value of P_4 was determined as follows:

First, the slip factor was estimated by computing a compressor work factor from the experimental data and subtracting the design windage factor of 0.039. (The effect that recalculating the windage factor based on experimental values of pressure and temperature had on the final value of P_3 was evaluated and dismissed as insignificant.) From estimated slip factor and impeller exit wheel speed, the fluid tangential velocity at the impeller exit was calculated. By assuming constant angular momentum between the impeller exit (station 3, fig. 9) and diffuser vane inlet (station 4, fig. 9), the tangential velocity at the diffuser vane inlet was calculated. The static temperature at the diffuser vane inlet was then determined by a simultaneous solution of three equations: (1) the continuity of mass flow, (2) the energy equation, and (3) the relation of the square of the absolute velocity being equal to the sum of the squares of the through flow and tangential velocities. In employing the continuity equation, the design effective through flow area was assumed. The design effective flow area was calculated from the design vector diagrams and measured passage widths. With the calculated static temperature, assumed total temperature, and measured static pressure at the diffuser vane inlet, the total pressure at this location was determined from the isentropic, perfect gas relation of pressure and temperature.

With the total pressure determined at the diffuser vane inlet (station 4, fig. 9), the total pressure at the impeller exit (station 3, fig. 9) was obtained based on the following iterative procedure. A loss coefficient for the radial vaneless diffuser section (stations 3 to 4, fig. 9) was employed in relating the total pressure at the impeller exit, P_3, to the total pressure at the diffuser vane inlet, P_4. The loss coefficient is defined as $P_3 - P_4$ divided by $P_3 - p_3$. A loss coefficient of 0.025 derived from the design values of pressures at stations 3 and 4 was employed in determining P_3. With the use of the design loss coefficient, the total pressure at the impeller exit was approximated based on $P_3 - p_3$ being approximately equal to $P_4 - p_4$. With the calculated tangential velocity and the estimated total pressure and measured total temperature at the impeller exit, the static temperature at the impeller exit was then determined by a simultaneous solution of the same three equations used to calculate the static temperature at station 4. In employing the continuity equation at station 3, the design effective through flow area at that location was assumed. With the calculated static temperature, measured total

temperature, and estimated total pressure at the impeller exit, the static pressure at this location was determined from the isentropic, perfect gas relation of pressure and temperature. With the static pressure thus determined at the impeller exit, a new total pressure at this location was calculated based on the design loss coefficient and the calculated value of $P_3 - p_3$. The iterations were repeated until a convergence was obtained on the calculated total pressure at the impeller exit. With the total pressure at the impeller exit thus determined, the impeller pressure ratio and impeller efficiency were then calculated.

REFERENCES

1. Stewart, Warner L.; Glassman, Arthur J.; and Krebs, Richard P.: The Brayton Cycle for Space Power. Paper No. 741 A, SAE, Sept. 1963.

2. Harrack, W. G.; and Caldwell, R. T.: System Optimization of Brayton-Cycle Space Power Plants. Paper No. 63-WA-87, ASME, Nov. 1963.

3. Anon.: Design and Fabrication of a High-Performance Brayton-Cycle Compressor Research Package. Rep. APS-5109-R, AiResearch Mfg. Co. (NASA CR-54368), May 1965.

4. Dollenback, F.: The Aerodynamic Design and Performance of Centrifugal and Mixed-Flow Compressors. Centrifugal Compressors. Tech. Prog. Ser., vol. 3, SAE, 1961.

NASA-Langley, 1968 —— 1 E-3645